Supplemental Information for

Twist engineering of the two-dimensional magnetism in double bilayer chromium triiodide homostructures

Hongchao Xie[1,+], Xiangpeng Luo[1,+], Gaihua Ye[2,+], Zhipeng Ye[2], Haiwen Ge[3], Suk Hyun Sung[4], Emily Rennich[5], Shaohua Yan[6], Yang Fu[6], Shangjie Tian[6], Hechang Lei[6], Robert Hovden[4], Kai Sun[1], Rui He[2,*], & Liuyan Zhao[1,*]

[1] Department of Physics, University of Michigan, 450 Church Street, Ann Arbor, MI, 48109, USA
[2] Department of Electrical and Computer Engineering, Texas Tech University, 910 Boston Avenue, Lubbock, TX, 79409, USA
[3] Department of Mechanical Engineering, Texas Tech University, 2703 7th Street, Lubbock, TX 79409, USA
[4] Department of Materials Science and Engineering, University of Michigan, 2300 Hayward Street, Ann Arbor, MI, 48109, USA
[5] Department of Mechanical Engineering, University of Michigan, 2350 Hayward Street, Ann Arbor, MI, 48109, USA
[6] Department of Physics and Beijing Key Laboratory of Opto-electronic Functional Materials & Micro-Nano Devices, Renmin University of China, Beijing, 100872, China

[*] Email: rui.he@ttu.edu; lyzhao@umich.edu
[+] These authors contributed equally

Table of Contents

S1. Theoretical calculations for determining the out-of-plane magnetic order in tDB CrI_3

Background preparations

Because the polar magneto-Raman geometry (i.e., normal incidence and backscattering geometry with the out-of-plane magnetic field) used in the current experiment, one could only access the out-of-plane components of spins due to the optical selection rule. Therefore, in our model analysis below, we will only focus on the out-of-plane components of spins. In principle, the frustration among spins in moiré magnets could result in spin canting off the out-of-plane direction even in Ising-type magnets [1]. While we do not explicitly include possible in-plane components in our model, it is worthwhile pointing out that the main conclusions from the model calculations below are not sensitive to the presence or absence of spin canting off the out-of-plane direction and are compatible with the noncollinear magnetism.

In a moiré superlattice, the periodic modulations of the interlayer stacking geometry lead to the magnetic domain structures in twisted CrI_3 [2]. While the structural stacking pattern and the resulting magnetic domain structure are sophisticated, it has been shown theoretically that two types of stacking geometries, AB (i.e., rhombohedral) and AB' (monoclinic) stacking, have the lowest elastic energy [3], and therefore, shall be the dominant ones. Instead of trying to capture all microscopic details about the stacking pattern and the lattice reconstruction, in our theory model, we will take a simplified setup and only focus on the most relevant and dominant parts: the monoclinic AB' and the rhombohedral AB stacking, while omitting the other high-energy stacking configurations. In reality, these high-energy stacking area may arise and fill up the regions other than the monoclinic and rhombohedral areas, especially at twist angles greater than $\sim 1.0^o$ [2]. But, the omission of them is sufficient to the leading order approximation.

In the twisted double bilayer (tDB) CrI_3 samples studied in our current work, the interlayer exchange coupling within individual bilayer (2L) CrI_3 remains antiferromagnetic (AFM), just the same as that in regular isolated 2L CrI_3, for which we take the value from the literature, $J_1 = 0.04\ \mathrm{meV}/\mu_B^2$ [2,3]. The coupling between the two 2L CrI_3 (i.e., at the interface between the two 2L CrI_3) requires the consideration of two types of structural stacking: monoclinic AB' stacking that corresponds to interlayer AFM exchange coupling and rhombohedral AB stacking that has interlayer ferromagnetic (FM) exchange coupling. We again adopt the values from literature [2,3], $J_1 = 0.04\ \mathrm{meV}/\mu_B^2$ for AFM and $J_2 = -0.6\ \mathrm{meV}/\mu_B^2$ for FM. Please note that, according to the first-principles calculations [2,3], $|J_2|$ is significantly greater than $|J_1|$. As it will be shown later, this fact is crucial for the development of net magnetization in the tDB CrI_3 with intermediate twist angles. Finally, the intralayer exchange coupling is known to be FM ($J < 0$) and the first-principles calculations give $J = -2.2\ \mathrm{meV}/\mu_B^2$.

Theoretical modeling in tDB CrI_3

For the monoclinic inter-bilayer stacked regions, the interlayer coupling between any two neighboring layers are all AFM with $J_1 = 0.04\ \mathrm{meV}/\mu_B^2$, and therefore its magnetism favors the interlayer AFM order: ↑↓↑↓ or ↓↑↓↑ from the top to the bottom layer. In contrast, for the rhombohedral inter-bilayer stacked regions, the preferred spin alignment is ↑↓↓↑ or ↓↑↑↓ because of the FM exchange coupling at the bilayer-bilayer interface. *It is important to note that for both stacking geometries, all these energetically favored spin configurations have zero net magnetization*. In the other word, neither of the stacking favors the development of a net magnetization that is observed in our experiment: *the large Raman circular dichroism for the 1.1^o twisted tDB CrI_3 at 0 T*. As we shall see below, to achieve the experimentally observed net

magnetization in 1.1° tDB CrI_3 at 0T, it requires the frustrated spin interactions due to the competition of spins between the monoclinic AFM and the rhombohedral FM regions.

- **the magnetic state with a zero total magnetization**

Case I: One very obvious possible configuration is that the monoclinic region has ↑↓↑↓ (or the opposite one), whereas the rhombohedral domain has ↑↓↓↑ (or the opposite one). In this configuration, each stacking region has its lowest-energy configuration, but the boundaries between them have opposite spin alignments within each of the bottom two layers. The energy penalty associated with such (intralayer) magnetic domain walls is proportional to the length of the domain boundary L multiplied by a factor of 2 because of their presence in two layers and the intralayer FM exchange coupling J, i.e., $E_1 \propto 2JL/a$ where a is the lattice constant of CrI_3. Because the intralayer coupling strength is much greater than the interlayer ones, this energy penalty will become large and dominant, when the domain boundary becomes long.

Case II: If the energy cost for such intralayer domain boundaries becomes too high, the system will favor a different configuration, i.e., avoiding any intralayer magnetic domain boundaries. Take an extreme case example, if the area of the monoclinic domain is much larger than the rhombohedral one, we would expect ↑↓↑↓ for both monoclinic and rhombohedral stacking regions. This spin configuration does not have any intralayer domain wall penalty, although the rhombohedral one is not in its ground state and is subject to the energy penalty of $E_2 \propto |J_2| (L/a)^2$, where L is the length of the domain boundary and the area shall scale with L^2.

Depending on the size of the domain L, which is controlled by the twisting angle of tDB CrI_3, the relative ratio between E_1 and E_2 shall change correspondingly. Most importantly, when the domain size is large (small), we shall expect $E_1 \ll E_2$ ($E_1 \gg E_2$), and thus the spin configuration shall follow the first (second) possibilities described above. Here, we emphasize again that all these spin configurations have zero total magnetization.

- **the magnetic state with a non-zero net magnetization**

Case III: For the intermediate domain size, where $E_1 \sim E_2$, new possible spin configuration can arise, for example, ↑↓↑↓ for the monoclinic region and ↑↑↑↓ for the rhombohedral region. In this case, the rhombohedral region is not in its ground state, because the top two layers (i.e., the top 2L CrI_3) both have spin up that is in contrast with the interlayer AFM coupling for a 2L CrI_3. This results in an energy penalty of $\sim J_1 (L/a)^2$. At the same time, the intralayer magnetic domain boundary only exists within one layer (i.e., the 2nd layer), which costs an energy of $\sim JL/a$. Therefore, in total, the energy cost for such a spin configuration is $E_3 \propto J_1 (L/a)^2 + JL/a$. Please note that this configuration has only one layer with intralayer magnetic domain wall (in the 2nd layer), so its intralayer energy cost is less than the Case I spin configuration where two layers are subject to intralayer magnetic domain wall (in the 3rd and 4th layers). This is the reason why this Case III configuration is possible to be more energetically favored than the Case I spin arrangement. In comparison to the Case II spin configuration, this Case III configuration has smaller interlayer energy cost, because $J_1 < |J_2|$.

This Case III spin configuration contains both intralayer and interlayer energy penalty (E_3), but the intralayer part is smaller than that of Case I (E_1) and the interlayer one is smaller than that of Case II (E_2). Therefore, when $E_1 \sim E_2$, this configuration could be most energetically favored.

- **the comparison of energies for the three spin configurations**

Below we compare the energies of these three configurations (Case I, II, and III) as a function of the domain size L. Here, we assume that the monoclinic region is greater, because it is the natural stacking for few-layer CrI_3. Here, we use L to represent the linear size of the rhombohedral stacking region (normalized by the lattice constant a), and L^2 to represent its corresponding area. In reality, it should be multiplied by a geometric factor of order 1, which depends on the shape and other geometrical details of the moiré superlattices, and this factor is set to 1 here for simplicity. At a qualitative level, our conclusion is robust to the exact value of this factor. For a similar argument, we set the length of the magnetic domain boundary to be $4L$.

With this setup and the approximations, we find that the energies of the three spin configurations described above are: $E_1 \approx 8\,J\,L$, $E_2 \approx |J_2|L^2$ and $E_3 \approx 4\,J\,L + J_1 L^2$. The values of J, J_1 and J_2 are obtained from first-principles calculations as mentioned in "background preparation" section [2,3]: $J = -2.2$ meV/μ_B^2, $J_1 = 0.04$ meV/μ_B^2, and $J_2 = -0.6$ meV/μ_B^2.

From Fig. S1, we can see that there are two critical lengths, L_1 (~ $4J/J_1$) and L_2 as marked, at which the most energetically favored spin configuration alters. Let's discussion the three regions below, above L_1, between L_1 and L_2, and below L_2.

(a) Above L_1 when the rhombohedral region dominates over the monoclinic region (i.e., not quite practical – the parameter range where this simple model fails when the twist angle is so big that the inter-bilayer coupling becomes so weak), the most energetically favored spin configuration is Case I: the monoclinic region has ↑↓↑↓ (or the opposite one) and the rhombohedral domain has ↑↓↓↑ (or the opposite one). This gives zero total net magnetization.

(b) Between L_1 and L_2 when the rhombohedral and monoclinic regions are comparable (i.e., intermediate twist angle), the most energy-saving spin configuration is Case III: the monoclinic region has ↑↓↑↓ and the rhombohedral domain has ↑↑↑↓. This configuration gives a finite total net magnetization, which is consistent with our result in the 1.1° tDB CrI_3.

(c) Below L_2 when the monoclinic region dominates over the rhombohedral region (i.e., very small twist angle), the most energetically favored spin configuration is Case II: homogeneous across the monoclinic and rhombohedral regions ↑↓↑↓. This again gives zero total net magnetization.

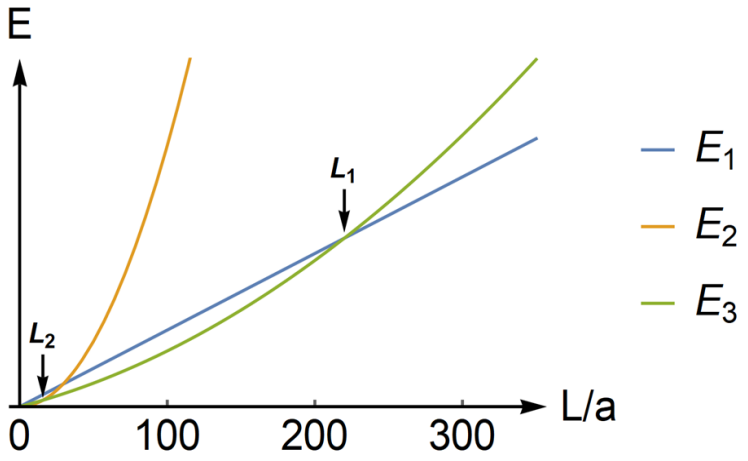

Figure S1 Plots of calculated energy penalty (E_1, E_2, and E_3) for the three spin configurations as a function of the rhombohedral stacking region size, normalized to the lattice constant a, i.e., L/a.

- **the consistency between calculations and experiment for the 1.1° tDB CrI_3**

We can do a quantitative comparison between our theoretical calculations and experimental observation. It should be emphasized due to the complicated nature of this material, we made approximations and simplifications in the theory treatment above. In addition, our theory has no fitting parameter at all, and the values of all control parameters are obtained from first-principles calculations. On the other hand, for small energy scales, like interlayer spin exchange, first-principles techniques are limited by resolution and accuracy, which is another source of error for our predicted values. Hence, the theory predicted values here should be treated as an order of magnitude estimation, instead of an exact solution.

With these limitations in mind, here we give key values from the theory predictions. The Case III spin configuration with a net magnetization shall arise at the critical domain size of $L_1 \approx 4J/J_1$. Using values from first-principles calculations [2,3], $L \approx 220$. This value is expected to scale with the linear size of a moiré unit cell. For our intermediate angle at which we observed Case III in the experiment, $\theta = 1.1°$, we expect $L \approx 1/\theta \approx 52$, which satisfies the requirement of $L < L_1$ and on the right order of magnitude with L_1.

Moreover, because the rhombohedral region has net magnetization, under an external magnetic field along (against) the direction of this net magnetization, the magnetic domain for the rhombohedral stacking shall increase (shrink) in size to reduce the energy. This magnetic domain size change is a smooth function of the magnetic field strength, and this is the reason why the signal intensity observed in this phase can vary continuously, gradually as the magnetic field increases.

S2. Calculations of the magnetism-coupled phonon contributions in tDB CrI_3

In few-layer CrI_3, it has been established that the interlayer structural coupling can lead to Davydov splitting of the A_g phonon mode of CrI_3, and these split phonon multiplets have two contributions in the Raman scattering: the pure structural and layered magnetism-coupled phonon contributions that correspond to the fully symmetric and antisymmetric Raman tensors [4]. Here, the layered magnetism-coupled phonon contribution encodes the static magnetic order information and tracks its evolution as a function of external magnetic field.

Here, we exploit the same idea for the strongly coupled 2L-2L regions, including both the monoclinic and rhombohedral inter-2L stacking regions, in tDB CrI_3. We perform the same analysis as in Ref. 4 to compute the magnetism-coupled phonon contributions for the various magnetic orders in the two stacking regions in different magnetic field ranges. The results are summarized in Table. S1 below.

Please note that the atomic displacement eigenvectors are nearly identical for the monoclinic and rhombohedral stacking regions, sharing the same symmetry properties although having slightly different atomic displacement magnitudes across the layers. Therefore, they are listed with the same sketch in Table. S1.

Table S1. Magnetism-phonon coupling strength ($\boldsymbol{U}_i \cdot \boldsymbol{M}^{\boldsymbol{M/R}}$) between the phonon mode ($\boldsymbol{U}_i$) and the magnetic order ($\boldsymbol{M}^{\boldsymbol{M/R}}$) in either monoclinic (M in the superscript, red) or rhombohedral (R in the superscript, blue) stacking regions in tDB CrI_3, across all four magnetic field regions with different out-of-plane spin configurations. In each entry,√ (×) stands for the presence (absence) of the magnetism-phonon coupling.

Modes / Magnetic States	$\boldsymbol{U}_1^{\mathrm{t}}$	$\boldsymbol{U}_2^{\mathrm{t}}$	$\boldsymbol{U}_3^{\mathrm{t}}$	$\boldsymbol{U}_4^{\mathrm{t}}$
$B_\perp < B_{\mathrm{C1}}^{\mathrm{R}}$, $\boldsymbol{M}^{\mathrm{M}} = \begin{bmatrix}1\\-1\\1\\-1\end{bmatrix}$	×	√	×	√
$B_\perp < B_{\mathrm{C1}}^{\mathrm{R}}$, $\boldsymbol{M}^{\mathrm{R}} = \begin{bmatrix}1\\1\\1\\-1\end{bmatrix}$	√	√	√	√
$B_{\mathrm{C1}}^{\mathrm{R}} < B_\perp < B_{\mathrm{C1}}^{\mathrm{M}}$, $\boldsymbol{M}^{\mathrm{M}} = \begin{bmatrix}1\\-1\\1\\-1\end{bmatrix}$	×	√	×	√
$B_{\mathrm{C1}}^{\mathrm{R}} < B_\perp < B_{\mathrm{C1}}^{\mathrm{M}}$, $\boldsymbol{M}^{\mathrm{R}} = \begin{bmatrix}1\\1\\1\\1\end{bmatrix}$	√	×	×	×
$B_{\mathrm{C1}}^{\mathrm{M}} < B_\perp < B_{\mathrm{C2}}$, $\boldsymbol{M}^{\mathrm{M}} = \begin{bmatrix}1\\-1\\1\\1\end{bmatrix}$	√	√	√	√
$B_{\mathrm{C1}}^{\mathrm{M}} < B_\perp < B_{\mathrm{C2}}$, $\boldsymbol{M}^{\mathrm{R}} = \begin{bmatrix}1\\1\\1\\1\end{bmatrix}$	√	×	×	×
$B_\perp > B_{\mathrm{C2}}$, $\boldsymbol{M}^{\mathrm{M}} = \begin{bmatrix}1\\1\\1\\1\end{bmatrix}$	√	×	×	×
$B_\perp > B_{\mathrm{C2}}$, $\boldsymbol{M}^{\mathrm{R}} = \begin{bmatrix}1\\1\\1\\1\end{bmatrix}$	√	×	×	×

References

1 Hejazi, K., Luo, Z.-X. & Balents, L. Noncollinear phases in moiré magnets. *Proceedings of the National Academy of Sciences* **117**, 10721, doi:10.1073/pnas.2000347117 (2020).

2 Wang, C., Gao, Y., Lv, H., Xu, X. & Xiao, D. Stacking Domain Wall Magnons in Twisted van der Waals Magnets. *Physical Review Letters* **125**, 247201, doi:10.1103/PhysRevLett.125.247201 (2020).

3 Sivadas, N., Okamoto, S., Xu, X., Fennie, C. J. & Xiao, D. Stacking-Dependent Magnetism in Bilayer CrI_3. *Nano Letters* **18**, 7658-7664, doi:10.1021/acs.nanolett.8b03321 (2018).

4 Jin, W. *et al.* Tunable layered-magnetism–assisted magneto-Raman effect in a two-dimensional magnet CrI_3. *Proceedings of the National Academy of Sciences* **117**, 24664, doi:10.1073/pnas.2012980117 (2020).